Modulations of interlayer exchange coupling through ultrathin MgO-based magnetic tunnel junctions: First-principles study

Shizhuo Wang,[1,2,3] Ke Xia,[2] Tai Min,[4,*] and Youqi Ke[1,†]

[1]*School of Physical Science and Technology, ShanghaiTech University, Shanghai 201210, China*
[2]*The Center for Advanced Quantum Studies and Department of Physics, Beijing Normal University, Beijing 100875, China*
[3]*College of Physics and Electronic Engineering, Zhengzhou University of Light Industry, Zhengzhou 450002, China*
[4]*Center for Spintronics and Quantum System, School of Materials Science and Engineering, Xi'an Jiaotong University, Xi'an 710049, China*

Ultrathin MgO-based magnetic tunnel junction (MTJ) features high electron/heat current density, presenting important applications in spintronics. Here, we report a first-principles study of the interlayer exchange coupling (IEC) through ultrathin MgO-based MTJs. We investigate the effects of different modulations on the IEC, including temperature, different interfacial disorders, and the type and thickness of the ferromagnetic (FM) materials. It is found that the interfacial disorders, such as oxygen vacancies, boron and carbon impurities, can significantly influence the magnitude and sign of the IEC. The presence of interfacial disorders enhances the anti-FM coupling contribution and reduces the FM coupling contribution to the total IEC, and can thus change the total IEC from FM to Anti-FM in the ultrathin MTJ. We also find that FM materials have important effects on IEC: the IEC with CoFe alloy exhibits much weaker dependence on the interfacial disorders and temperature than that with the Fe. Our first-principles results provide a good explanation for the serious inconsistency between previous experimental measurements. Moreover, by studying the junction structure Vacuum/FM1/MgO/FM2 (FM1, FM2=Fe, CoFe), we find that the ultrathin FM1 layers can dramatically enhance the FM IEC and the IEC enhancement significantly depends on the combination of FM1-FM2. We show that the enhanced FM IEC with ultrathin FM1 can be sustained with a considerable amount of surface roughness in FM1 and interfacial disorder.

I. INTRODUCTION

MgO-based magnetic tunnel junctions (MTJ) have attracted great research interest in the field of spintronics because of its important technological applications such as spin-torque diode [1], high-frequency oscillator [2], and especially the application in magnetic random access memory (MRAM) cells [3–5]. The merit of the MgO-based MTJ lies in the distinct resistance states depending on the relative magnetization direction of the two ferromagnetic (FM) electrodes, i.e., typically, the parallel (P) configuration presents resistance significantly lower than the antiparallel (AP) configuration [6]. The essence of information storage based on MTJ is the magnetic switching between the P and AP configurations of the magnetization. Instead of using an external magnetic field, the magnetic switching in MTJ could be realized by two important mechanisms as proposed recently: the first is the spin transfer torque induced by a spin-polarized current with applied bias [7–11]; the second is the sizable thermal spin torque (TST) induced by a heat current with applied temperature gradient [12–16]. For the spin torque in MTJs, the spin-polarized current or heat current contribute comparably to the in-plane ($T_\parallel$) and out-of-plane ($T_\perp$) components of the spin torque, which are both important for magnetic switching and precession in MTJs [14,17,18]. In the MTJ FM1/MgO/FM2, besides the electron/heat current induced spin torque, the spins in the two FM materials can interact through the interlayer exchange coupling (IEC), providing an important contribution to $T_\perp$ and thus affecting the magnetic processing in an

operating MTJ [19]. However, in previous first-principles studies of spin torque in MTJ devices, the IEC contribution is not considered [14,20–22]. Usually, IEC is negligible in MTJs with a thick insulting barrier because of its exponential decay with increasing barrier thickness [23,24]. However, the IEC contribution to spin torque can become significant and play an important role in magnetic switching in thin-barrier MTJs that feature high electron/heat current density. Presently, various device properties of thin MTJs have been intensively studied by experiments and theories [14–16,24–29]. Very importantly, in an ultrathin MTJ with 0.9-nm MgO, the magnetic switching assisted by grand TST has been experimentally observed recently, stimulating more research interest in ultrathin MTJs [15]. Therefore, for magnetic switching in thin MgO-based MTJs, it is important to study the IEC and its different modulations.

Presently, the IEC through MgO-based MTJs has been extensively studied by experiments [23–28]. However, the experimental results are not consistent with each other. For example, the IEC energies in Fe/ MgO/Fe MTJs reported in Refs. [25] and [26] have very large discrepancies in the magnitude and sign. In particular, in Ref. [25], the maximal strength of antiferromagnetic (AFM) IEC measured is about -0.26 erg/cm^2 in 0.5-nm-MgO MTJ, while in Ref. [26], the maximal AFM IEC is as small as -0.045 erg/cm^2 in 0.65-nm-MgO MTJs and the IEC even exhibits a ferromagnetic (FM) coupling for a 0.5-nm-MgO MTJ. These large discrepancies between Refs. [25] and [26] have been attributed to a large concentration of oxygen vacancies (OVs) in the device [26]. Moreover, in contrast to the AFM IEC observed in the thin Fe/MgO/Fe MTJ, IEC in ultrathin CoFe(B)/MgO/CoFe (B) MTJs presents only FM coupling as reported in Refs. [23,24]. Recent experiments have demonstrated that the sign and

---

*tai.min@xjtu.edu.cn
†keyq@shanghaitech.edu.cn

strength of IEC can be significantly influenced by the annealing and measured temperature [28]. Therefore it is generally believed that the disorders, such as OVs and impurities, which vary from sample to sample, play important roles in the IEC of ultrathin MTJs. For example, Ref. [27] reported that the IEC in the ultrathin MgO-based MTJ can be significantly reduced by the interfacial diffusive carbon impurities. Beside the modulation of the IEC by disorder, the IEC through ultrathin MTJ may also be modulated by changing the thickness of the magnetic layers [30], similar to the oscillating IEC in a magnetic multilayer with a metallic spacer [31–35]. On the theoretical side, many phenomenological modes for studying IEC in MTJ [31,32,36] have been proposed with tunable parameters, but cannot be applied to study the disorder effects at nanoscale. To study the ultrathin nanoscale MTJ with disorders, it requires first-principles method with the effective treatment of disorder configurational average on the physical properties. Up to date, first-principles studies of IEC in disordered MgO-based MTJ [26,29,37] have demonstrate the AMF IEC meditated by oxygen vacancies based on supercell total energy calculations. In these calculations [26,29,37], the disorder is handled by supercell method with very large disorder concentration and the IEC energy is obtained as total energy difference between P and AP configurations. However, the disorder average requires performing calculations over all the possible disorder configurations, thus is difficult to be modeled by several supercell calculations. In this paper, we report a first-principles study of the IEC in ultrathin MgO-based MTJs with the disorder average treated by an analytical method. We demonstrate the important effects of different modulations on the IEC including temperature, different interfacial disorders, and type and thickness of the FM materials. Two different MTJ structures, including FM/MgO/FM and Vacuum/FM1/MgO/FM2, are used in our first-principles study of the MTJ.

This paper is organized as follows. In Sec. II, we introduce the first-principles method to calculate the IEC in disordered MTJs with disorder average treated analytically; in Sec. III, we present the IEC results for the MTJ FM/MgO/FM (FM = Fe, $Co_{0.5}Fe_{0.5}$) and investigate the effects of barrier thickness, temperature, interfacial disorders including OVs, boron and carbon. In Sec. IV, we present the IEC results for the MTJ structure Vacuum/FM1/MgO/FM2 (FM1, FM2 = Fe, $Co_{0.5}Fe_{0.5}$) and discuss the effects of FM1 and FM2 materials, the FM1 thickness and disorders on the IEC. Finally, we conclude our studies in Sec. V.

II. METHODS AND NUMERICAL DETAILS

Here, we adopt the surface-Green's-function (SGF) technique to compute the IEC within the well-established first-principles framework of tight-binding linear muffin-tin orbital (TB-LMTO) approach [38–42]. As shown in Fig. 1(a), we consider two-probe device structures in which a central device region containing disorders is sandwiched by two semi-infinite electrodes, such as the two structures shown in Figs. 1(b) and 1(c).

Generally, the IEC energy of the disordered structure of Fig. 1(a) can be defined as

$$J(\theta) = \overline{\Omega}(\theta) - \overline{\Omega}(0), \qquad (1)$$
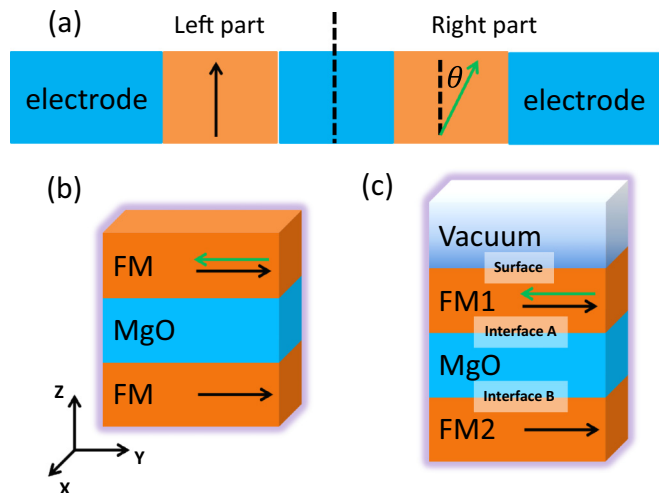

FIG. 1. (a) Sketch of a two-probe device containing a central region sandwiched by two electrodes: the relative angle between the magnetization of the two FM layers (orange colored) is θ, the dotted line at the center separates the system into left and right parts; (a) MTJ with a tunnel barrier sandwiched by two semi-infinite FM electrodes; (b) MTJ with a tunnel barrier sandwiched by FM1 with finite thickness and semi-infinite FM2. The FM materials considered include Fe and $Co_{0.5}Fe_{0.5}$ alloy.

where the overbar denotes the configurational average over disorders and $\Omega(\theta)$ is the grand canonical potential for the structure with the relative angle θ between the two magnetization directions of the electrodes [39–41]. In Eq. (1), $J > 0$ and $J < 0$ denote the FM and AFM IECs, respectively. From Ref. [39], we know, in TB-LMTO method, the averaged grand canonical potential can be given as follows:

$$\overline{\Omega}(\theta) = -\frac{1}{\pi}\text{Im}\int_C f(z)\text{tr}\overline{\ln g^\alpha(\theta,z)}\,dz, \qquad (2)$$

in which $f(z)$ is the Fermi-Dirac distribution function and g^α is the auxiliary Green's function of the system in the α representation [38]. Here, direct computation of the disorder averaged $\overline{\ln g^\alpha(\theta,z)}$ involves very difficult vertex corrections. To go further, one can rewrite $\overline{\ln g^\alpha(\theta,z)} = \ln \overline{g^\alpha}(\theta,z) - X$, where $X = \overline{\ln g^\alpha} - \ln \overline{g^\alpha}$ includes the nontrivial vertex corrections. Very importantly, it has been proven that the vertex correction X depends very weakly on the variable θ. Thus the IEC energy can be rewritten as

$$J(\theta) = -\frac{1}{\pi}\text{Im}\int_C f(z)\text{tr}[\ln \overline{g^\alpha}(\theta,z) - \ln \overline{g^\alpha}(0,z)]dz$$
$$= \frac{1}{\pi}\text{Im}\int_\Lambda \int_C f(z)\text{tr}\ln\left[1 - \frac{1-\cos(\theta)}{2}M(k_{||},z)\right]dz, \qquad (3)$$

where Λ denotes the 2D Brillouin zone (BZ), and the vertex corrections in $\overline{\Omega}(\theta)$ and $\overline{\Omega}(0)$ are canceled out, called "vertex cancellation theorem" [42]. Because the translational invariance is restored after the configurational average, the final result can be obtained with the Fourier transform by following the standard algebra in Ref. [41]. Then, the quantity

TABLE I. IEC strength (in unit of erg/cm^2) through FM/MgO(n ML)/FM (001) MTJ. The values in the bracket of the first column are the MgO barrier thickness in nanometers. 5% and 10% interfacial OVs are considered at both interfaces, the ambient temperatures (T) considered are 0 and 300 K.

n	T	Fe/MgO/Fe			CoFe/MgO/CoFe		
		clean	5% OV	10% OV	clean	5% OV	10% OV
2 (0.42 nm)	0 K	9.78	3.89	-2.48	7.43	5.57	3.11
	300 K	7.53	2.28	-3.17	7.35	5.49	3.03
3 (0.62 nm)	0 K	3.45×10^{-1}	1.06×10^{-1}	-2.19×10^{-1}	4.76×10^{-1}	4.04×10^{-1}	2.53×10^{-1}
	300 K	2.90×10^{-1}	2.90×10^{-2}	-2.45×10^{-1}	4.71×10^{-1}	3.99×10^{-1}	2.47×10^{-1}
4 (0.82 nm)	0 K	5.06×10^{-3}	-7.20×10^{-3}	-2.36×10^{-2}	4.24×10^{-2}	3.47×10^{-2}	2.29×10^{-2}
	300 K	3.13×10^{-4}	-1.19×10^{-2}	-2.46×10^{-2}	4.20×10^{-2}	3.44×10^{-2}	2.28×10^{-2}
5 (1.03 nm)	0 K	-6.25×10^{-4}	-1.58×10^{-3}	-2.83×10^{-3}	4.41×10^{-3}	4.13×10^{-3}	3.51×10^{-3}
	300 K	-7.08×10^{-4}	-1.64×10^{-3}	-2.71×10^{-3}	4.37×10^{-3}	4.11×10^{-3}	3.49×10^{-3}
6 (1.23 nm)	0 K	-1.47×10^{-4}	-1.90×10^{-4}	-2.42×10^{-4}	3.90×10^{-4}	4.03×10^{-4}	3.77×10^{-4}
	300 K	-1.41×10^{-4}	-1.80×10^{-4}	-2.22×10^{-4}	3.91×10^{-4}	4.04×10^{-4}	3.79×10^{-4}
7 (1.43 nm)	0 K	-1.96×10^{-5}	-2.35×10^{-5}	-2.86×10^{-5}	4.90×10^{-5}	5.33×10^{-5}	5.34×10^{-5}
	300 K	-1.81×10^{-5}	-2.17×10^{-5}	-2.64×10^{-5}	4.91×10^{-5}	5.35×10^{-5}	5.40×10^{-5}
8 (1.63 nm)	0 K	-2.38×10^{-6}	-2.43×10^{-6}	-2.32×10^{-6}	5.00×10^{-6}	6.11×10^{-6}	7.05×10^{-6}
	300 K	-2.17×10^{-6}	-2.19×10^{-6}	-2.07×10^{-6}	5.06×10^{-6}	6.21×10^{-6}	7.18×10^{-6}

M in the above equation can be given by

$$M = -\left(1 - S_{RL}^{\alpha} \overline{\mathcal{G}_L^{\uparrow}} S_{LR}^{\alpha} \overline{\mathcal{G}_R^{\uparrow}}\right)^{-1} S_{RL}^{\alpha} (\overline{\mathcal{G}_L^{\uparrow}} - \overline{\mathcal{G}_L^{\downarrow}})$$
$$\times \left(1 - S_{LR}^{\alpha} \overline{\mathcal{G}_R^{\downarrow}} S_{RL}^{\alpha} \overline{\mathcal{G}_L^{\downarrow}}\right)^{-1} S_{LR}^{\alpha} (\overline{\mathcal{G}_R^{\uparrow}} - \overline{\mathcal{G}_R^{\downarrow}}), \quad (4)$$

where, to use the SGF technique, the device is divided into the left (L) and right (R) subsystems as shown in Fig. 1(a). In the above equation, the structure constants matrix $S_{RL/LR}^{\alpha}$ denotes the coupling of the neighboring principle layers between the left and right subsystems, and $\overline{\mathcal{G}}_{L/R}^{\sigma}$ are the configurational averaged SGF of the left/right part for the spin σ [38]. To compute the averaged SGF, the coherent potential approximation (CPA) [43–45] is applied in combination with the renormalization-decimation technique [46]. After obtaining the matrix M for each $k_{||}$ and contour energy z, the IEC energy can be computed by the integration of Eq. (3). Consequently, the effects of different modulations can be analyzed from first principles.

In all our first-principles simulations, the electronic structure is self-consistently computed with density functional theory by using the von Barth-Hedin LSDA exchange-correlation functional [47]. Hence the effects of charge transfer enhancement of magnetic moments at the interface and interfacial states can be well included in calculating the IEC. The MTJs that we studied here consist of a MgO barrier sandwiched by two FM materials, such as the two different structures in Figs. 1(b) and 1(c). The structure lattices are periodic in the $x-y$ plane and z corresponds to the growth direction along the (001) direction of *bcc* lattice structure of the Fe or CoFe alloy FM material. We use the experimental lattice constant 2.866 Å for FM layers and neglect all the lattice distortions due to disorders and the lattice mismatch between FM/MgO (see Refs. [14,48,49] for more details). In this paper, we only present the results of the IEC energy for $\theta = \pi$, while obtaining the results for arbitrary θ is straightforward with Eq. (3) since the M matrix is independent of θ. To calculate M in Eq. (4), we choose the central position of MgO

barrier as the boundary to partition the system into two parts. For the disorders, we consider the CoFe alloys, interfacial impurities/defects, such as OVs, carbon, and boron impurities with different concentrations. For the contour integration in Eq. (3), a semicircle contour of diameter 2.5 Ry is used with energy points generated by the Gaussian quadrature method. We use 35 contour energy points for the calculations at zero temperature, and additional 24 points for the finite-temperature calculation to include the effects of occupied states above E_F and Matsubara energies (the poles on the complex plane) [50]. For the 2D BZ integration, 200×200 $k_{||}$ points are sampled to ensure the convergence for IEC calculation.

III. IEC IN FM/MGO/FM

In this section, we present the IEC results for Fe/MgO/Fe (Fe-MTJ) and CoFe/MgO/CoFe (CoFe-MTJ) as sketched in Fig. 1(b), and we discuss the IEC energy dependence on the MgO barrier thickness, ambient temperature, and interfacial disorders (OVs, carbon and boron impurities).

As shown in Table I, we first study the IEC dependence on the MgO thickness for the Fe- and CoFe-MTJs with different concentrations of interfacial OVs at 0 and 300 K. It can be found that the IEC amplitude decreases exponentially with increasing MgO thickness, as observed in experiments [23,24]. This is because the transmission of the electrons carrying magnetic information decays exponentially with increasing barrier thickness, resulting in fast decrease in the magnetic coupling between the two FM electrodes. According to the phenomenological model [36], for the MTJs with thick barrier, the dependence of IEC energy (J) on barrier thickness (d) could be given by the relation $J \propto \exp(-2\kappa d)$, where the parameter κ denotes the decaying speed of IEC values. By fitting the IEC strength of CoFe-MTJ with 6–8-MLs MgO, we obtain $\kappa = 0.52$ and 0.49 Å^{-1} for junctions with the respective clean and 10%OV disordered interfaces, and the κ in Fe-MTJ are very close to the value of CoFe-MTJ. Our result

for κ agrees well with the result of total energy simulation [37] $\kappa = 0.55 \text{ Å}^{-1}$ and is comparable to the experimental result [23] $\kappa = 0.40 \text{ Å}^{-1}$. In experiments, the IEC gives rise to the hysteresis-loop field shift H_s, which could be given as $H_s = \frac{J}{t_F M_s}$ [24,26,28], where t_F is the thickness of free FM layers, M_s is the saturation magnetization of the free layer. Adopting the parameters ($t_F = 2.3$ nm and $M_s = 0.8M$ A/m) used in Ref. [24], the IEC energy 0.035 erg/cm^2 (for CoFe/MgO(4 ML, 0.82 nm)/CoFe MTJ with interfacial 5%OV in Table I) corresponds to the hysteresis-loop field shift $H_s = 190$ Oe in experiment.

Although the exponential decay of the IEC with increasing MgO thickness is not determined by the FM materials and interfacial disorders, the FM materials and interfacial disorders do have significant effects on the sign and magnitude of IEC. As shown in Table I, as increasing the OV concentration, for Fe-MTJs, the IEC can change from FM to AFM for MgO less than 5 MLs, or always remain AFM but negligible for MgO thicker than 5 MLs. However, for all the calculated CoFe-MTJs, the increment of interfacial OVs only decreases the FM coupling strength without changing the sign. The FM IEC in disordered CoFe-MTJs reflects the fact that the diffusive scattering in the CoFe alloy opens more channels for the FM coupling between two electrodes, compared to the Fe electrodes. This large difference in the sign of IEC between Fe- and CoFe-MTJs is consistent with the experimental findings in Refs. [25,26] and Refs. [23,24], respectively. Our calculations reveal the general trend that interfacial OVs enhance the AFM coupling and weaken the FM coupling contribution to total IEC, agreeing well with supercell simulations [29,37] and the experiments [26]. In particular, the IEC energy in clean Fe/MgO(3ML)/Fe is 0.35 erg/cm^2 (0 K), which can be reduced by almost three times to 0.11 erg/cm^2 by introducing 5% interfacial OVs and even changes the sign to become -0.22 erg/cm^2 by 10% OVs (the same magnitude as the clean MTJ).

In addition to FM materials and disordered OV, we also investigate the temperature effects in Table II. By comparing the results of 0 and 300 K, we can see that the temperature effects on IEC in Fe-MTJs are much larger than in CoFe-MTJs. More apparently, in the ultrathin Fe-MTJ, increasing temperature decreases the FM coupling, but favors the AFM coupling. For detailed studies, we present the results for the IEC energy versus temperature in Fig. 2, where the interested 3-ML-MgO junctions are shown, the IEC dependence on temperature in Fe-MTJ is obvious in Fig. 2(a), while the IECs in all the simulated CoFe-MTJ are only very slightly decreased with increasing temperature as shown in Fig. 2(b). In particular, in Fe-MTJ, compared to the values at T = 0 K, the FM coupling for MTJ with 5% OV can be reduced by 78% at 300 K, and the AFM coupling for MTJ with 10% OV can be increased by 26% at 250 K, while the maximal IEC decrease in CoFe-MTJ is only 2.5%. Furthermore, it should be emphasized that an important feature in Fig. 2 is that the effect of interfacial OVs on IEC is much more significant than the temperature effects for both Fe- and CoFe-MTJs.

Except the OVs in MgO, boron and carbon impurity atoms are also observed at the FM/MgO interface in experiments [27,51–53]. In realistic MTJ samples, the types and concentra-
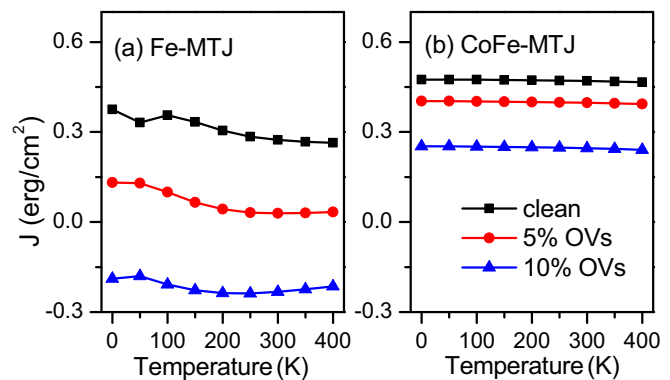

FIG. 2. Temperature-dependent IEC through FM/MgO(3 ML)/FM MTJs with different interfacial disorders: clean (black-square), 5% OV (red-circle), and 10% OV (blue-triangle). (a) is for Fe-MTJs and (b) is for CoFe-MTJs.

tions of interfacial disorders are closely related to the specific fabrication conditions. By scanning the disorder concentration at both interfaces in 3-ML-MgO MTJs, we show how the IEC energy depends on the disorders in Fe and CoFe junctions in Fig. 3. The disorder types considered here include OVs, diffused boron, and carbon atoms in place of oxygen in the MgO layer adjacent to interfaces. We can clearly see that, for all the disorder types, increasing the disorder concentration favors the AFM coupling and decreases the FM coupling. For all the MTJs calculated, the strongest AFM coupling can be found in the Fe-MTJ with interfacial carbon impurities. Moreover, we can find that all three types of disorders show much weaker effects in the CoFe-MTJ than in the Fe-MTJ, demonstrating the important effects of the FM materials. For example, it is noticeable that for all the OV concentrations investigated, the CoFe-MTJ always remains FM coupling, while AFM IEC can be found in the Fe-MTJ, agreeing with the experiments in Refs. [23,24,26]. To provide a more detailed
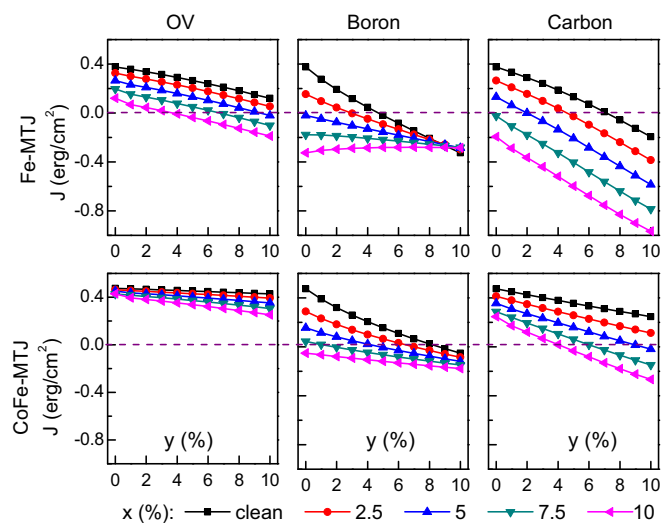

FIG. 3. IEC energy J (at 0 K) for FM/MgO(3 ML)/FM MTJs with three types of interfacial disorders, including OV, boron and carbon impurities (presented in the first, second, and third columns, respectively). The disorder concentration is indexed by $x\%$ ($y\%$) for the left (right) interface.
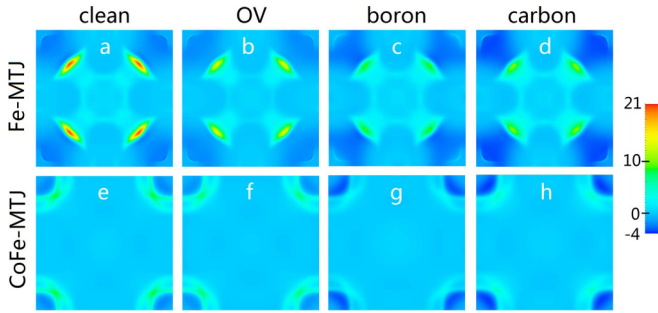
FIG. 4. $k_{||}$-resolved IEC (erg/cm^2) for FM/MgO(3 ML)/FM MTJs with different interfacial disorders including OV, boron, and carbon impurities. We consider the disorder concentration 5% at both interfaces. (a)–(d) are for Fe-MTJs and (e)–(h) are for CoFe-MTJs.

understanding of the disorder effects on IEC, we plot the $k_{||}$-resolved IEC for Fe- and CoFe-MTJs with interfacial OVs, and boron and carbon impurities in Fig. 4.

As shown in Fig. 4, the $k_{||}$-resolved IEC energy exhibits very different patterns in Fe- and CoFe-MTJs. In particular, the FM coupling is more diffusive in CoFe-MTJs than in Fe-MTJs. In Fe-MTJs, we can observe the "hot spots" with FM coupling localized in certain areas of the 2D BZ, especially in perfect Fe-MTJs. However, by introducing disorders in Fe-MTJs, one could find the amplitude of the IEC hot spots is quickly reduced, and the AFM coupling is enhanced (see the blue areas at the corner of BZ in Fig. 4). It is apparent that the carbon impurity is the most effective in reducing FM coupling and enhancing AFM coupling, giving rise to the quickest decrease in total IEC energy with carbon in Fig. 3.

IV. IEC IN VACCUM/FM1/MGO/FM2

Here, by using the Vac/FM1(n ML)/MgO(3 ML)/FM2 sur-MTJ structure as shown in Fig. 1(c), we investigate the important effects of finite thickness of FM1 on the IEC energy. In our calculation, we found that, due to the important quantum confinement effect, the spin density of state of the single-layer FM1 is significantly modulated compared to the bulk and interfacial FM1 materials. Thus we would expect different IEC in the MTJs with ultrathin FM1 in comparison with the MTJs with the semi-infinite FM materials discussed in the last section. Due to the geometrical asymmetry of the structure and large differences in Fe and CoFe as thin FM1 materials, we calculate IEC in the MTJs with four different combinations of Fe and CoFe as FM1 and FM2 materials. In Fig. 5(a), we plot IEC dependence on the thickness of FM1 in perfect MTJs at T = 0 K. Most apparently, the ultrathin FM1 material can significantly enhance the FM IEC compared to MTJs with thicker or semi-infinite FM1. In particular, for $n = 1$, IEC energies, for the respective FM1-FM2 combinations of Fe-CoFe, CoFe-Fe, Fe-Fe, and CoFe-CoFe, are 349%, 160%, 143%, and 56% larger than that of the MTJs with semi-infinite FM1. By increasing the FM1 material thickness, all the IEC energies are decreased quickly to the values of the junctions with semi-infinite FM1 materials. Another obvious feature in Fig. 5 is that the IEC results oscillate with the thickness of the FM1 and the oscillation amplitude decays quickly as increasing FM1 thickness. This IEC oscillation can be

attributed to the interference of the quantum well states [31] in the finite FM1 material. For $n > 4$, we can see the IEC energies are only slightly changed for the four cases, converging to the results of MTJs with semi-infinite FM1. Thus we can see the IEC strength in the calculated MTJs is mostly determined by the 1-nm-thick FM materials next to the interfaces. In Fig. 5(a), for $n = 1$, we can also find the very distinct IEC strength with different FM1-FM2 combinations.

To understand this significant FM material dependence of the IEC, we plot the IEC versus energy (below Fermi energy) Y(z) in Fig. 5(b) for the four FM1-FM2 combinations. Here, the $Y(z)$ is obtained as

$$Y(z) = \text{Im} \sum_{k_{||}} w(k_{||}) \text{tr} \ln \left[1 - \frac{1 - \cos(\theta)}{2} M(k_{||}, z) \right]. \quad (5)$$

The integration $J = \frac{1}{\pi} \int_C f(z) Y(z) \, dz$ gives the total IEC. To obtain the smooth $Y(z)$ curves in Fig. 5(b), we add 10^{-4} Ry as the imaginary part to z in all the calculations. In Fig. 5(b), we find all the IEC spectra exhibit both FM and AFM coupling at different energies and the FM coupling dominates, providing the large FM IEC in all the sur-MTJs. For the four MTJs, the IEC spectra curves are quite different from each other. These differences are given by the different spin states in the FM1 and FM2 materials. In Fig. 5(b), the largest FM IEC energy in Fe-CoFe MTJ can be attributed to the significantly enhanced FM coupling in a large energy range near the Fermi energy compared to other sur-MTJs. Whereas, in the CoFe-CoFe junction, we observe an AFM coupling peak and the narrow energy range for FM coupling near the E_F, resulting in the weakest FM IEC compared to others. Thus we can see the different combinations of FM1 and FM2 materials have important effects on the IEC energy. In Fig. 5(c), we plot the $k_{||}$-resolved IEC in the 2D BZ. It is clearly seen that the four corners of the BZ contributes strong FM coupling, in contrast to the AFM coupling found in the Fe- and CoFe-MTJs as shown in Fig. 4. The detailed distribution patterns of $k_{||}$-resolved IEC are different for the four junctions calculated. For the four junctions, very small regions in BZ exhibit AFM coupling. Most apparently, the Fe-CoFe junction presents the strongest FM coupling around the BZ corners compared to others. In particular, we can see the "hot" lines for FM coupling in Fe-CoFe junction and the maximum FM coupling amplitude is about 20.15 erg/cm^2. The existence of "hot" lines results in the total FM IEC as large as 2.0 erg/cm^2 in Fe-CoFe MTJs.

To understand the quantum confinement induced large enhancement effects in FM IEC in the sur-MTJs, we investigate the difference in the energy-resolved $Y(z)$ and $k_{||}$-resolved $J(k_{||})$ between the MTJs with 1 ML and semi-infinite FM1 materials, namely,

$$\Delta Y(z) = Y_{\text{FM1 (1 ML)}}(z) - Y_{\text{FM1 }(\infty)}(z), \quad (6)$$

$$\Delta J(k_{||}) = J_{\text{FM1 (1 ML)}}(k_{||}) - J_{\text{FM1 }(\infty)}(k_{||}). \quad (7)$$

In Fig. 6, we plot ΔY and ΔJ (in the inset) for Fe-CoFe and CoFe-Fe MTJs as examples. For the energy-resolved ΔY, large FM IEC enhancement is found within the range ~ 1 eV below E_F, contributing mostly to the total IEC energy
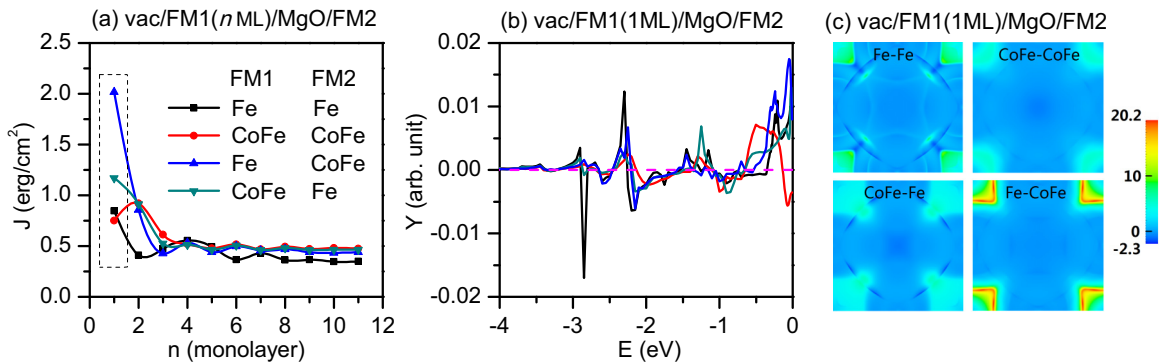
FIG. 5. (a) FM1 thickness dependence of the IEC in perfect Vac/FM1(n ML)/MgO/FM2 MTJs with four combinations of Fe and CoFe alloy as FM1 and FM2 materials. (b) Energy-resolved IEC Y [in Eq. (5)] for Vac/FM1(1 ML)/MgO/FM2 junction. (c) $k_{\parallel}$-resolved IEC (in unit of erg/cm^2) through Vac/FM1(1 ML)/MgO/FM2 MTJs.

difference between MTJs with ultrathin and semi-infinite FM1 materials. From the inset of Fig. 6, we can see the change in IEC is mostly concentrated around the corner of BZ, such as the "hot" line in the Fe-CoFe MTJ.

In the following, we study the effects of different disorders on the IEC in sur-MTJs, including the surface roughness and interfacial OV. For the surface roughness, it is represented by the alloy model Fe$_{1-x}$Va$_x$ (Va denotes vacuum sphere with the same radius as Fe). Figure 7 presents the IEC energy versus Va concentration x for Fe-CoFe and Fe-Fe MTJs. It is clearly seen that, as increasing x, the IEC energy in Fe-CoFe MTJs presents a fast decrease, while IEC in Fe-Fe MTJs changes much slower, even have a slight increase at small x. In particular, when $x = 20\%$, the IEC energies are 1.04 erg/cm^2 in Fe-CoFe MTJ and 0.80 erg/cm^2 in Fe-Fe MTJs, compared to 2.02 and 0.85 erg/cm^2 in the respective Fe-CoFe and Fe-Fe perfect MTJs. It should be mentioned that, in a large range of x, the IEC energies in both MTJs show important enhancement compared to the values of the MTJs with semi-infinite FMs. It can be seen that, with almost about 50% Va, the IEC energies in both MTJs can be decreased to the corresponding values with a semi-infinite FM1 layer.

The interfacial OV effects on IEC in sur-MTJs are shown in Fig. 8 for Fe-Fe and Fe-CoFe MTJs. Figure 8 plots the IEC energy versus the thickness of the FM1 materials. Since the structure of sur-MTJ is asymmetric, we here index the two interfaces as interface A (if-A) and interface B (if-B) as shown in Fig. 1(c). As shown, the interfacial OV decreases the FM coupling in both MTJs. For example, 5% (10%) OVs at if-A decrease the FM coupling strength by 6.9% (13.2%) compared to that in clean junction, while, for OV at if-B, the IEC is decreased by 10.9% (21.7%). It is notable that the effects of OV at if-A and -B depend on the FM materials used. Another important feature of IEC in Fig. 8 is that IEC strength oscillates with the number of FM1 layers. The oscillation can be explained as the "quantum interferences" inside the magnetic layers [30–32], which is the direct consequence of interference associated with the electron wave multiple reflections in a magnetic layer of finite thickness. In Fig. 8, by introducing interfacial disordered OV, we find an oscillation period slightly changed, but the IEC strength can be significantly reduced by disorders and this modulation depends on the used FM materials.
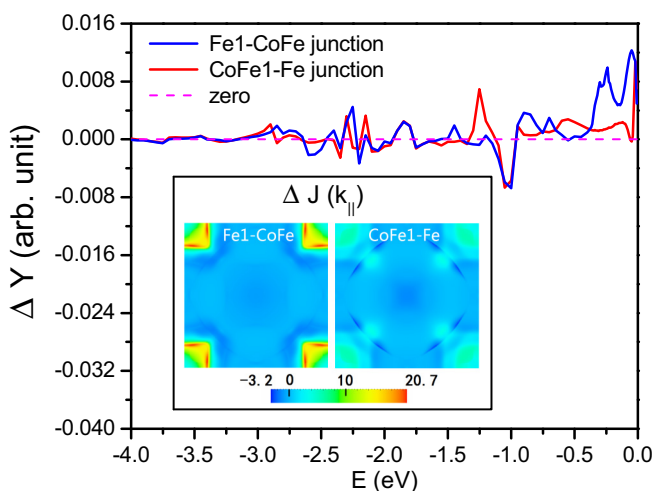

FIG. 6. Energy-resolved ΔY IEC difference between MTJs with one layer FM1 and semi-infinite FM1 layers. (Inset) $k_{\parallel}$-resolved IEC difference in the 2D BZ.
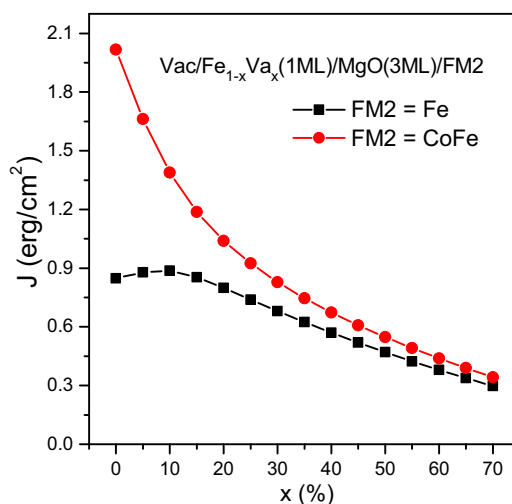

FIG. 7. IEC dependence on the surface roughness in Vac/Fe$_{1-x}$Va$_x$(1 ML)/MgO(3 ML)/FM2 MTJs, black-square line for FM2=Fe and red-circle line for FM2=CoFe.
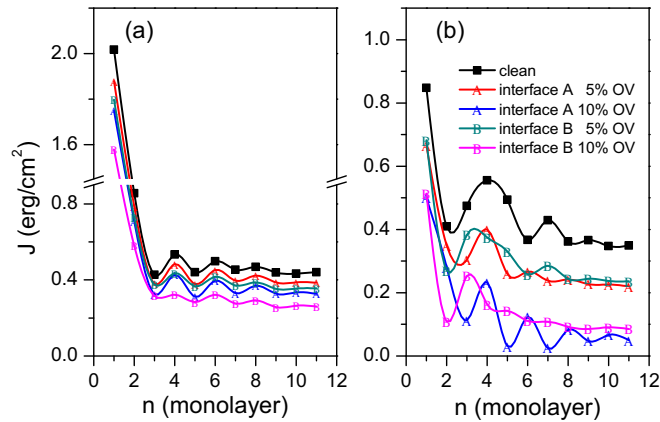
FIG. 8. IEC dependence on the thickness of FM1=Fe for MTJs with different concentrations of interfacial disordered OVs: (a) is for MTJs with FM2=CoFe and (b) is for MTJs with FM2= Fe.

V. SUMMARY

In summary, we have carried out a first-principles study of the IEC through ultrathin MgO-based MTJs. We demonstrate the important effects of different modulations of the IEC. The temperature shows much weaker effects than the interfacial disorders. The interfacial disorders such as oxygen vacancies, carbon, and boron impurities, can significantly reduce the FM coupling and enhance the AFM coupling contribution to the total IEC. As an important result, the magnitude and sign of IEC in MTJs can be substantially modulated by the disorders. We also find the use of FM materials is important for the IEC: the IEC with a CoFe alloy exhibits a much weaker dependence on the disorder and temperature than that with Fe. Furthermore, in the MTJs with the structure vacuum/FM1/MgO/FM2, we find the dramatic enhancement of the IEC with the ultrathin FM1 materials and the enhancement decreases quickly and exhibits oscillations with increasing the thickness of FM1. We show that the magnitude of the IEC enhancement significantly depends on the combination of FM1 and FM2 materials. It is found that the enhanced IEC with ultrathin FM1 can be sustained with a considerable amount of surface roughness in FM1 and interfacial disorder.

[1] A. A. Tulapurkar, Y. Suzuki, A. Fukushima, H. Kubota, H. Maehara, K. Tsunekawa, D. D. Djayaprawira, N. Watanabe, and S. Yuasa, Nature (London) **438**, 339 (2005).

[2] S. I. Kiselev, J. C. Sankey, I. N. Krivorotov, N. C. Emley, R. J. Schoelkopf, R. A. Buhrman, and D. C. Ralph, Nature (London) **425**, 380 (2003).

[3] S. S. P. Parkin, C. Kaiser, A. Panchula, P. M. Rice, B. Hughes, M. Samant, and S.-H. Yang, Nat. Mater. **3**, 862 (2004).

[4] S. Yuasa, T. Nagahama, A. Fukushima, Y. Suzuki, and K. Ando, Nat. Mater. **3**, 868 (2004).

[5] S. Ikeda, J. Hayakawa, Y. Ashizawa, Y. M. Lee, K. Miura, H. Hasegawa, M. Tsunoda, F. Matsukura, and H. Ohno, Appl. Phys. Lett. **93**, 082508 (2008).

[6] W. H. Butler, X.-G. Zhang, T. C. Schulthess, and J. M. MacLaren, Phys. Rev. B **63**, 054416 (2001).

[7] J. C. Slonczewski, J. Magn. Magn. Mater. **159**, L1 (1996); L. Berger, Phys. Rev. B **54**, 9353 (1996).

[8] E. B. Myers, D. C. Ralph, J. A. Katine, R. N. Louie, and R. A. Buhrman, Science **285**, 867 (1999).

[9] Y. Xu, K. Xia, and Z. Ma, Nanotechnology **19**, 235404 (2008).

[10] H. Kubota, A. Fukushima, K. Yakushiji, T. Nagahama, S. Yuasa, K. Ando, H. Maehara, Y. Nagamine, K. Tsunekawa, D. D. Djayaprawira, N. Watanabe, and Y. Suzuki, Nat. Phys. **4**, 37 (2008).

[11] C. Wang, Y.-T. Cui, J. A. Katine, R. A. Buhrman, and D. C. Ralph, Nat. Phys. **7**, 496 (2011).

[12] M. Hatami, G. E. W. Bauer, Q. F. Zhang, and P. J. Kelly, Phys. Rev. Lett. **99**, 066603 (2007).

[13] H. Yu, S. Granville, D. P. Yu, and J.-Ph. Ansermet, Phys. Rev. Lett. **104**, 146601 (2010).

[14] X.-T. Jia, K. Xia, and G. E. W. Bauer, Phys. Rev. Lett. **107**, 176603 (2011).

[15] A. Pushp, T. Phung, C. Rettner, B. P. Hughes, S.-H. Yang, and S. S. P. Parkin, Proc. Natl. Acad. Sci. USA **112**, 6585 (2015).

[16] J. C. Leutenantsmeyer, M. Walter, V. Zbarsky, M. Munzenberg, R. Gareev, K. Rott, A. Thomas, G. Reiss, P. Peretzki, H. Schuhmann, M. Seibt, M. Czerner, and C. Heiliger, SPIN **03**, 1350002 (2013).

[17] I. Theodonis, N. Kioussis, A. Kalitsov, M. Chshiev, and W. H. Butler, Phys. Rev. Lett. **97**, 237205 (2006).

[18] A. Brataas, A. D. Kent, and H. Ohno, Nat. Mater. **11**, 372 (2012).

[19] P. M. Haney, C. Heiliger, and M. D. Stiles, Phys. Rev. B **79**, 054405 (2009).

[20] X.-T. Jia, K. Xia, Y. Ke, and H. Guo, Phys. Rev. B **84**, 014401 (2011).

[21] C. Franz, M. Czerner, and C. Heiliger, Phys. Rev. B **88**, 094421 (2013).

[22] C. Heiliger, C. Franz, and M. Czerner, J. Appl. Phys. **115**, 172614 (2014).

[23] S. Serrano-Guisan, W. Skowronski, J. Wrona, N. Liebing, M. Czapkiewicz, T. Stobiecki, G. Reiss, and H. W. Schumacher, J. Appl. Phys. **110**, 023906 (2011).

[24] W. Skowroński, T. Stobiecki, J. Wrona, K. Rott, A. Thomas, G. Reiss, and S. van Dijken, J. Appl. Phys. **107**, 093917 (2010).

[25] J. Faure-Vincent, C. Tiusan, C. Bellouard, E. Popova, M. Hehn, F. Montaigne, and A. Schuhl, Phys. Rev. Lett. **89**, 107206 (2002).

[26] T. Katayama, S. Yuasa, J. Velev, M. Ye. Zhuravlev, S. S. Jaswal, and E. Y. Tsymbal, Appl. Phys. Lett. **89**, 112503 (2006).

[27] A. Kozioł-Rachwał, T. Ślęzak, M. Ślęzak, K. Matlak, E. Młyńczak, N. Spiridis, and J. Korecki, J. Appl. Phys. **115**, 104301 (2014).

[28] R. R. Gareev, V. Zbarsky, J. Landers, I. Soldatov, R. Schafer, M. Münzenberg, H. Wende, and P. Grünberg, Appl. Phys. Lett. **106**, 132408 (2015).

[29] H. X. Yang, M. Chshiev, A. Kalitsov, A. Schuhl, and W. H. Butlter, Appl. Phys. Lett. **96**, 262509 (2010).

[30] L. E. Nistor, B. Rodmacq, S. Auffret, A. Schuhl, M. Chshiev, and B. Dieny, Phys. Rev. B **81**, 220407(R) (2010).

[31] P. Bruno, Phys. Rev. B **52**, 411 (1995).

[32] P. Bruno, Europhys. Lett. **23**, 615 (1993).

[33] L. Nordström, P. Lang, R. Zeller, and P. H. Dederichs, Phys. Rev. B **50**, 13058(R) (1994).

[34] P. J. H. Bloemen, M. T. Johnson, M. T. H. van de Vorst, R. Coehoorn, J. J. de Vries, R. Jungblut, J. aan de Stegge, A. Reinders, and W. J. M. de Jonge, Phys. Rev. Lett. **72**, 764 (1994).

[35] S. N. Okuno and K. Inomata, Phys. Rev. Lett. **72**, 1553 (1994).

[36] J. C. Slonczewski, Phys. Rev. B **39**, 6995 (1989).

[37] M. Y. Zhuravlev, J. Velev, A. V. Vedyayev, and E. Y. Tsymbal, J. Magn. Magn. Mater. **300**, e277 (2006).

[38] I. Turek *et al. Electronic Structure of Disordered Alloys, Surfaces, and Interfaces* (Kluwer, Dordrecht, 1997).

[39] J. Kudrnovský, V. Drchal, I. Turek, and P. Weinberger, Phys. Rev. B **50**, 16105 (1994).

[40] V. Drchal, J. Kudrnovský, I. Turek, and P. Weinberger, Phys. Rev. B **53**, 15036 (1996).

[41] J. Kudrnovský, V. Drchal, P. Bruno, I. Turek, and P. Weinberger, Phys. Rev. B **54**, R3738 (1996).

[42] P. Bruno, J. Kudrnovský, V. Drchal, and I. Turek, Phys. Rev. Lett. **76**, 4254 (1996).

[43] B. Velický, S. Kirkpatrick, and H. Ehrenreich, Phys. Rev. **175**, 747 (1968).

[44] P. Soven, Phys. Rev. **156**, 809 (1967)

[45] B. Velický, Phys. Rev. **184**, 614 (1969).

[46] M. P. L. Sancho, J. M. L. Sancho, and J. Rubio, J. Phys. F: Met. Phys. **15**, 851 (1985).

[47] U. von Barth and L. Hedin, J. Phys. C: Solid State Phys. **5**, 1629 (1972).

[48] Y. Ke, K. Xia, and H. Guo, Phys. Rev. Lett. **105**, 236801 (2010).

[49] S.-Z. Wang and K. Xia, Phys. Rev. B **93**, 184414 (2016).

[50] K. Wildberger, P. Lang, R. Zeller, and P. H. Dederichs, Phys. Rev. B **52**, 11502 (1995).

[51] C. Tiusan, M. Sicot, J. Faure-Vincent, M. Hehn, C. Bellouard, F. Montaigne, S. Andrieu, and A. Schuhl, J. Phys.: Condens. Matter **18**, 941 (2006).

[52] Y. F. Chiang, J. J. I. Wong, X. Tan, Y. Li, K. Pi, W. H. Wang, H. W. K. Tom, and R. K. Kawakami, Phys. Rev. B **79**, 184410 (2009).

[53] J. C. Read, P. G. Mather, and R. A. Buhrman, Appl. Phys. Lett. **90**, 132503 (2007).